Support Information

Ferrocenyl Carboxylate-Mediated Electrode/Electrolyte Dual-Phase Molecule Engineering for Efficient and Durable Electrochemical Oxygen Evolution Reaction

Xuetong Zhang, Chong Lin*, Ye Tan, Cuiping Zeng, Xinyi Luo, Hongshun Deng, Ke Li, Min Li, Jingyang Tian*, Minghui Cao*

[a.] *Jiangxi Province Key Laboratory of Functional Organic polymers, School of Chemistry and Materials Science, East China University of Technology, Nanchang, 330013, Jiangxi, P. R. China.*

Experimental Details

Reagents and Materials

Metal precursor of nickel nitrate hexahydrate ($Ni(NO_3)_2 \cdot 6H_2O$, 99.5%) was supplied by Shanghai Aladdin Biochemical Technology Co., Ltd. Organic alkali of hexamethylenetetramine (HMT, 99.5%) was provided by Shanghai Titan Scientific Co., Ltd. Electrolyte of potassium hydroxide (KOH, 95%) was obtained from Shanghai Macklin Biochemical Co., Ltd. Sulfur source of thiourea (CH_4N_2S, 99%) and selenium source of selenium powder (Se, 99.9%) were purchased from Beijing InnoChem Science & Technology Co., Ltd. The modifier of 1,1'-Ferrocenedicarboxylic acid ($H_2FeC_{12}H_{10}O_4$, FcDA, ≥ 98.0%) was obtained from TCI (Shanghai) Development Co., Ltd. The solvents of anhydrous methanol (AR), anhydrous ethanol (AR), N, N-dimethylformamide (DMF, AR) were supplied by Xilong Technology Co., Ltd. All analytical reagent grade chemicals are commercially available without further purification. Carbon cloth (CC, WOS1009, thickness: 0.33 mm) was purchased from CeTech Co. Ltd.

Material preparation

Preparation of $Ni(OH)_2$ NAs

1 mmol $Ni(NO_3)_2 \cdot 6H_2O$ and 2 mmol HMT were dissolved in 30 mL anhydrous methanol. The solution was then transferred into a Teflon lining (100 mL), and a piece of washed CC or NF (3 cm × 3 cm) was put into the solution. Subsequently, the Teflon-lined stainless-steel autoclave was heated at 120 °C for 24 h. The obtained $Ni(OH)_2$ NAs were washed with deionized water and anhydrous ethanol several times, and were dried at 60 °C for further use.

Preparation of $Ni(OH)_2$-FcDA NAs

In a typical preparation of $Ni(OH)_2$-FcDA NAs, moderate FcDA was ultrasound dissolved in the mix solvents of 8 mL DMF and 4 mL H_2O. Then, the solution was transferred into a 25 mL Teflon-lined stainless-steel autoclave. At the same time, a piece of as-prepared $Ni(OH)_2$ NAs (3 cm × 1 cm) were placed in the solution. Then, the autoclave was heated to 125 °C for 24 h. The obtained $Ni(OH)_2$-FcDA NAs were washed with were washed with deionized water and ethanol several times, and were dried at 60 °C for further use.

Materials characterizations

The structure of the samples was characterized by X-ray diffraction (XRD) (Bruker AXS D8 Advance) with Cu Kα radiation. Fourier transform infrared spectroscopy

(FTIR, Thermo Nicolet iS50 FT-IR spectrometer) was used to qualitatively analyze the functional groups. The resolution and total scan numbers were 4 cm^{-1} and 64, respectively. The morphologies of the samples were characterized by field emission scanning electron microscopy (FE-SEM, Nova Nano SEM 450) and transmission electron microscopy (TEM, Tecnai G2 F20 S-Twin). Raman spectroscopy studies were conducted using a Renishaw inVia ReflexRaman microscope equipped with a 532 nm laser source. The energy dispersive X-ray spectroscopy (EDX) was used for elemental analysis. X-ray photoelectron spectroscopy (XPS) was recorded on a X-ray photoelectron spectrometer (Thermo Fisher ESCALAB Xi+ spectrometer) with Al Kα X-ray source.

Electrochemical measurements

All the electrochemical measurements were tested by a CHI 760E electrochemical workstation at room temperature (25 °C). A standard three-electrode system was used in all the electrochemical tests. A Pt plate and a Hg/HgO electrode (in 1 M KOH) were used as the counter and reference electrodes, respectively. $Ni(OH)_2$ NAs and $Ni(OH)_2$-FcDA NAs (0.5 cm × 1.0 cm) were used as the working electrodes. The electrolyte was 1 M KOH with or without 25 μM FcDA, which was degassed by bubbling oxygen for 30 min before measurements. All potentials were referenced to a reversible hydrogen electrode (RHE) using the equation: $E_{vs.RHE} = E_{vs.Hg/HgO} + 0.098\ V + 0.059 \times pH$. All linear sweep voltammetry (LSV) data for OER performance evaluation were acquired via a reverse scan (from high to low potential) at a scan rate of 5 mV s^{-1}. The reverse scan direction was deliberately chosen to avoid the interference of the oxidation current from Ni^{2+}/Ni^{3+} redox processes on the intrinsic water oxidation current, thereby providing a more accurate assessment of the OER activity. All LSV data presented are with positive feedback iR compensation (95% compensation) applied, and this compensation procedure was applied consistently to all tested samples and under all electrolyte conditions. The overpotential at 10 mA cm^{-2} (η_{10}) was calculated as $\eta_{10} = E_{vs.RHE}@10\ mA\ cm^{-2} - 1.23\ V$. The Tafel slope was derived by fitting the η *vs*. log(j) plot with the Tafel equation ($\eta = blogj + a$). Electrochemically active surface area (ECSA) was estimated from the double-layer capacitance (C_{dl}) measured via cyclic voltammetry (CV) in a non-Faradaic potential region (1.0-1.1 V vs. RHE) at various scan rates (100-5000 mV s^{-1}). Chronopotentiometry (CP) tests were performed at a constant current density of 10 mA cm^{-2}.

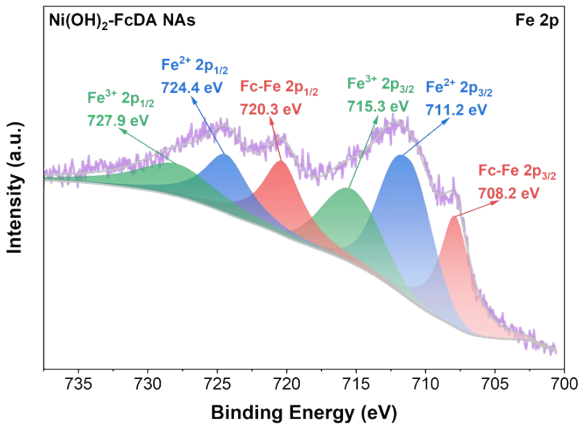

Figure S1. XPS of Fe 2p in $Ni(OH)_2$-FcDA NAs.

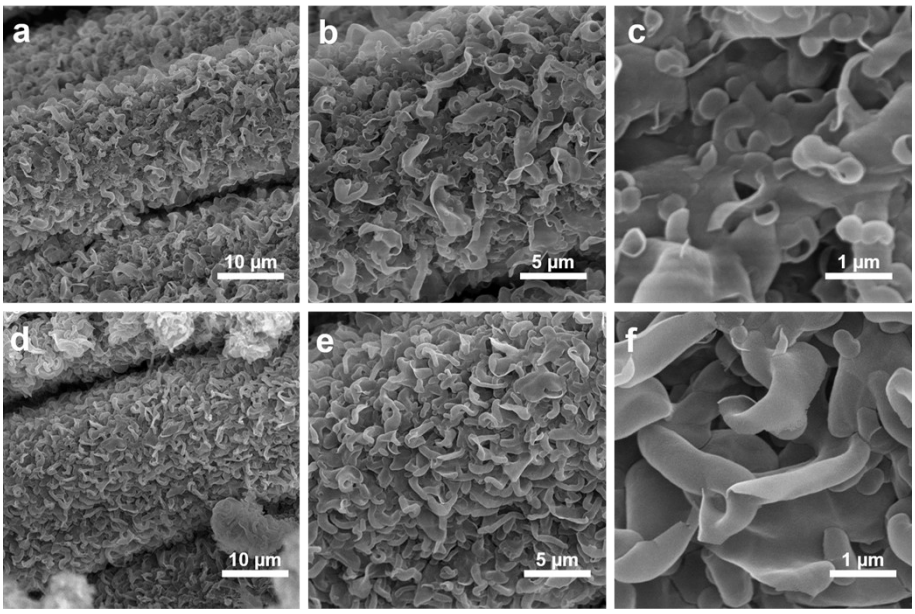

Figure S2. SEM images of (a-c) $Ni(OH)_2$ NAs, (d-f) $Ni(OH)_2$-FcDA NAs, respectively.

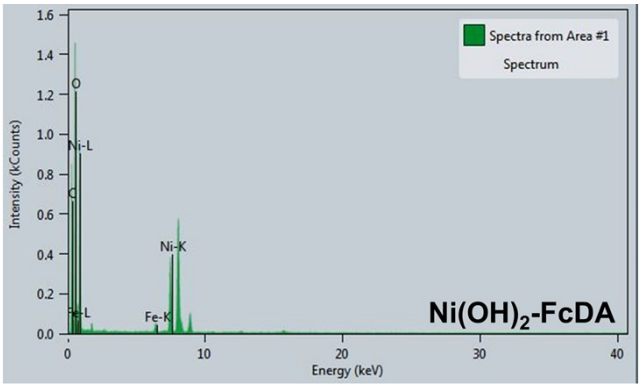

Figure S3. EDS plots of (a) $Ni(OH)_2$-FcDA.

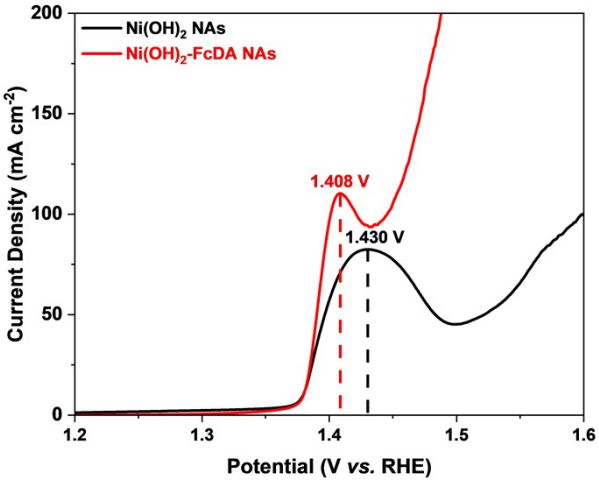

Figure S4. Forward scanned LSV curves of (a-c) $Ni(OH)_2$ NAs, and (d-f) $Ni(OH)_2$-FcDA NAs under the electrolyte of 1 M KOH.

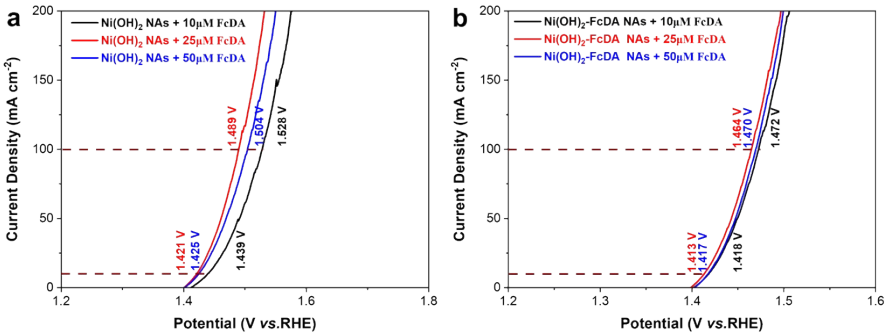

Figure S5. LSV curves of $Ni(OH)_2$ NAs and $Ni(OH)_2$-FcDA NAs at different FcDA concentration in 1M KOH.

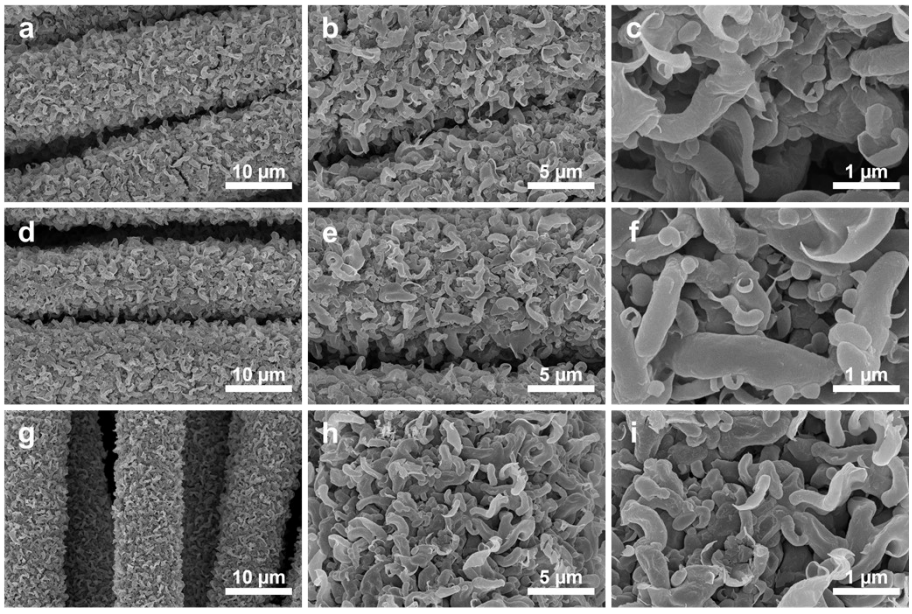

Figure S6. SEM images of $Ni(OH)_2$ NAs following activation in 1 M KOH solution for 2 hours, with the inclusion of 10 μM (a–c), 25 μM (d–f), and 50 μM (g–i) FcDA.

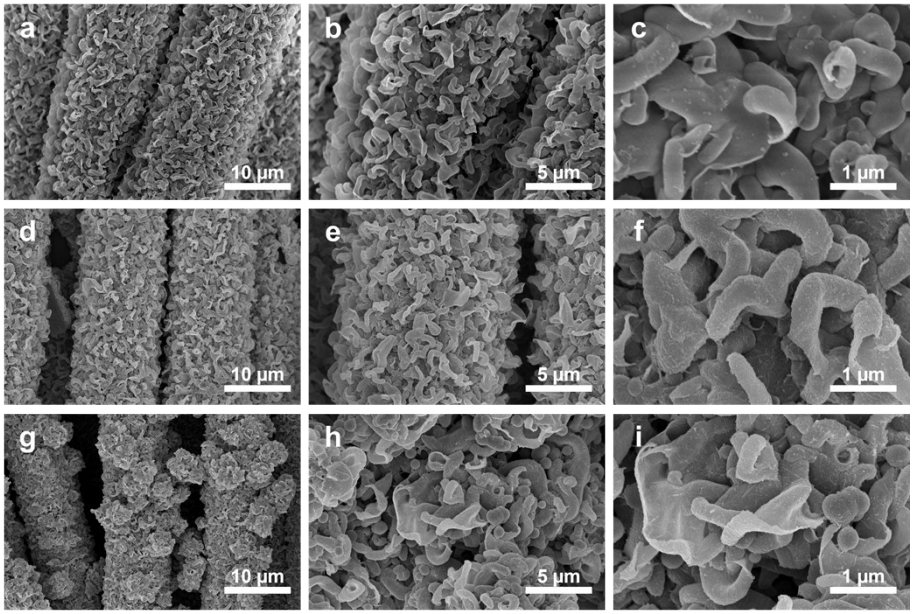

Figure S7. SEM images of $Ni(OH)_2$-FcDA NAs following activation in 1 M KOH solution for 2 hours, with the inclusion of 10 μM (a–c), 25 μM (d–f), and 50 μM (g–i) FcDA.

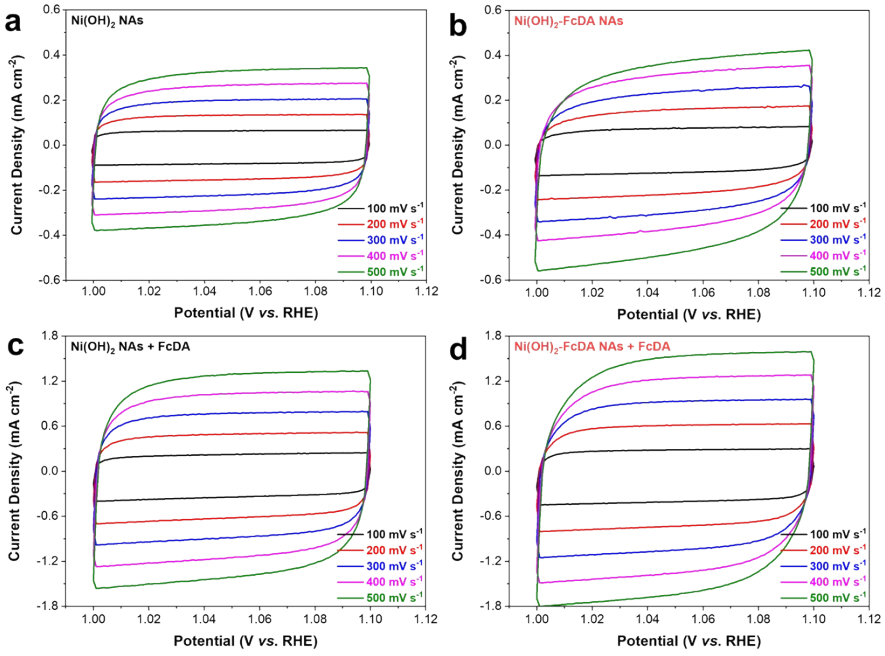

Figure S8. CV curves of (a) $Ni(OH)_2$ NAs, (b) $Ni(OH)_2$-FcDA NAs at various scan rates in the electrolyte of KOH solution; CV curves of (c) $Ni(OH)_2$ NAs and (d) $Ni(OH)_2$-FcDA NAs at various scan rates in the electrolyte of FcDA in KOH solution.

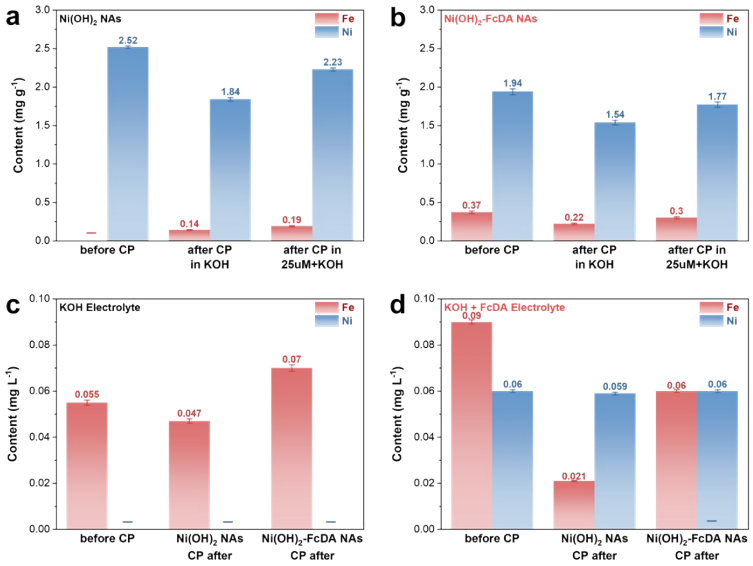

Figure S9. Ni and Fe contents in (a) $Ni(OH)_2$ NAs and (b) $Ni(OH)_2$-FcDA NAs electrodes before and after CP tests. (c, d) Concentrations of Ni and Fe leached into the electrolyte after stability testing, as determined by ICP-OES.

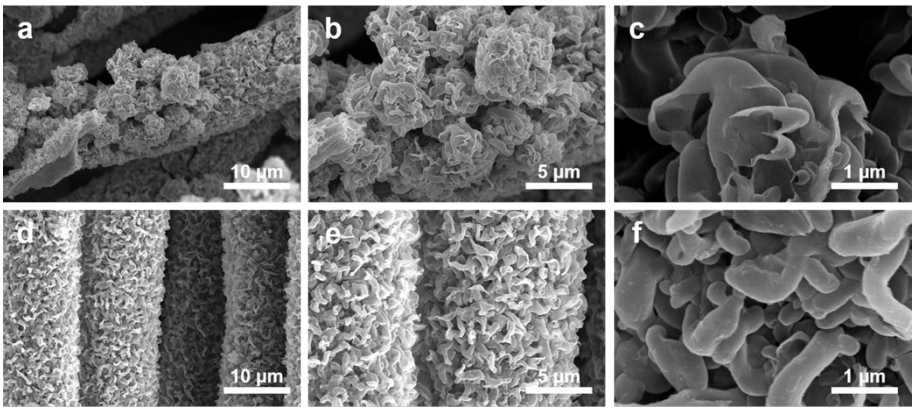

Figure S10. SEM images of (a-c) $Ni(OH)_2$ NAs, and (d-f) $Ni(OH)_2$-FcDA NAs after CP test in the electrolyte of KOH solution.

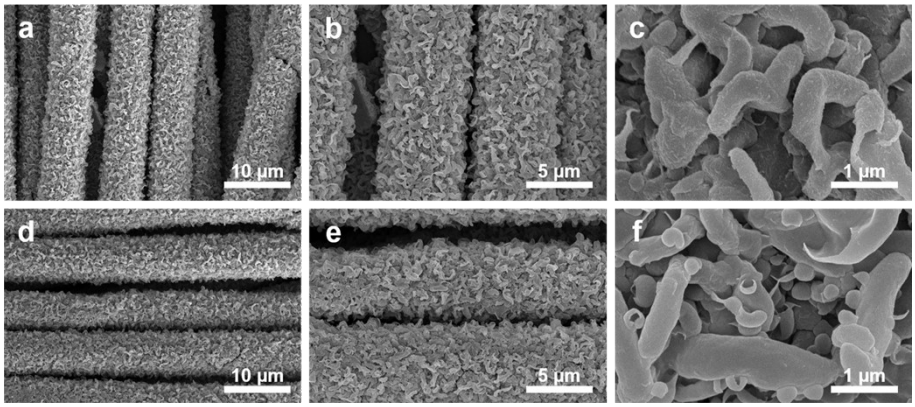

Figure S11. SEM images of (a-c) $Ni(OH)_2$ NAs, and (d-f) $Ni(OH)_2$-FcDA NAs after CP test in the electrolyte of 25 μM FcDA in 1 M KOH solution.

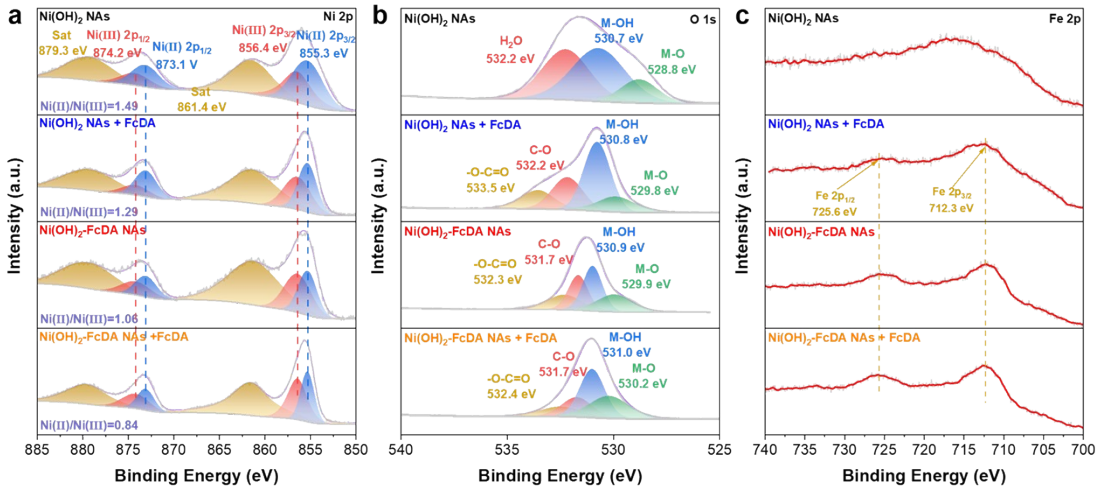

Figure S12. XPS of (a) Ni 2p, (b) O 1s and (c) Fe 2p in $Ni(OH)_2$ NAs and $Ni(OH)_2$-FcDA NAs after CP tests in the electrolyte of KOH solution and in the electrolyte of moderate FcDA in KOH solution.

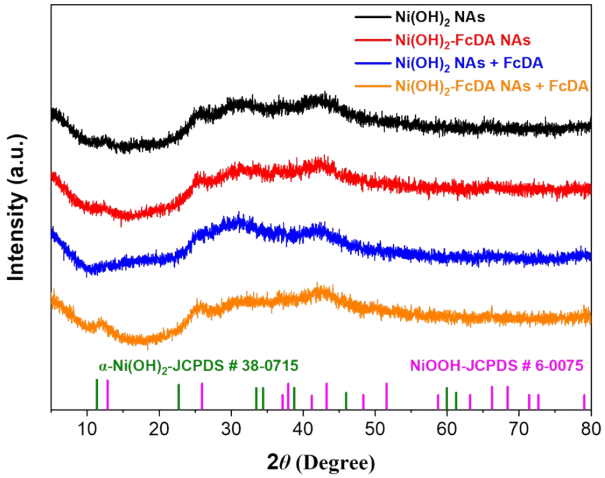

Figure S13. XRD of $Ni(OH)_2$ NAs and $Ni(OH)_2$-FcDA NAs after CP test.

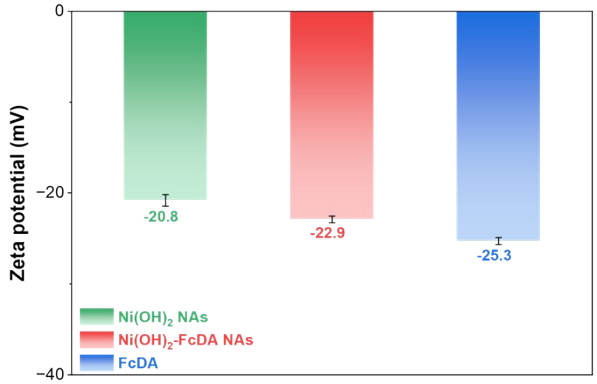

Figure S14. The results of zeta potential test of $Ni(OH)_2$-FcDA NAs compared with the $Ni(OH)_2$ NAs and FcDA at pH = 14.

Table S1. Comparison of Catalytic OER Performance in Alkaline Electrolytes.

Electrocatalysts	η_{10} (mV)	Tafel slope (mV dec^{-1})	Reference
$Ni(OH)_2$-FcDA NAs	**203**	**38.2**	**This work**
$Ni(OH)_2$ NAs + CL	**194**	**82.1**	**This work**
$Ni(OH)_2$ NAs-FcDA NAs+ CL	**183**	**53.2**	**This work**
Fe-$NiSe_2$(V_{Se}-$Ni_{0.70}Fe_{0.30}Se_2$)	210	61	[1]
Ce-NiO-E	382	118.7	[2]
NiO-$NiFe_2O_4$/rGO	296	43	[3]
Sm-NiO-E	409	81	[4]
$NiSe_2$@Fe-NiCo LDH	260	108.9	[5]
Fe-$NiSe_2$($Fe_{0.2}Ni_{0.8}Se_2$)	242	68	[6]
Co-$NiSe_2$($Co_{0.13}Ni_{0.87}Se_2$/Ti)	320	94	[7]
m-$Ni_{0.94}Fe_{0.06}Se_2$	279	39	[8]
Cu-(a-NiSe/c-$NiSe_2$)/TiO_2 NRs	339	54.2	[9]
$Ni_{0.7}Fe_{0.3}Se_2$-30% rGO	265	57	[10]
Fe-$NiSe_2$-25($Fe_{0.5}Ni_{0.5}Se_2$)	250	52	[11]
NiFe(2,2'-bpy)$_2$@CNT	240	42.4	[12]
a-CoPSe	223	32	[13]
Fe^{2+}-NiFe LDH	249	40.3	[14]
$NiCo_{2-x}Fe_xO_4$ NBs	274	42	[15]
30% Ce-NiFe-LDH	242	34	[16]
NiFe LDH-UF	254	32	[17]
HG-NiFe	310	39	[18]
Fe-doped-(Ni-MOFs)/FeOOH	210	50	[19]
FeOOH@NiFe LDH(0.2 M)	252	51.5	[20]
Ni-MIL-53-Fc	297	60.2	[21]
NiFe LDH nanomesh	268	30	[22]
FeNi LDH sheet/FeNi	130	39	[23]
NiFeV LDHs	192	42	[24]
$Ni_{0.67}Fe_{0.33}$/C	210	35	[25]
CoFe LDH HNC	238	42	[26]

The table compares the catalytic OER performance of three key systems developed in this work: (1) $Ni(OH)_2$-FcDA NAs in 1 M KOH, (2) $Ni(OH)_2$ NAs in 1 M KOH with

50 μM FcDA additive, and (3) $Ni(OH)_2$-FcDA NAs in 1 M KOH with 50 μM FcDA additive. Their performance, evaluated by metrics such as the overpotential at 10 mA cm^{-2} (η_{10}) and Tafel slope, is benchmarked against other state-of-the-art Ni-based electrocatalysts reported in the literature (Ref S1-S26), with all data obtained in KOH-based electrolytes for a fair comparison.

Reference

(1) Hassan, M. H.; Soliman, A. B.; Elmehelmey, W. A.; Abugable, A. A.; Karakalos, S. G.; Elbahri, M.; Hassanien, A.; Alkordi, M. H. A Ni-loaded, metal–organic framework–graphene composite as a precursor for *in Situ* electrochemical deposition of a highly active and durable water oxidation nanocatalyst. *Chem. Commun.,* 2019, ***55*** (1), 31–34.

(2) Gao, W.; Xia, Z.; Cao, F.; Ho, J. C.; Jiang, Z.; Qu, Y. Comprehensive understanding of the spatial configurations of CeO_2 in NiO for the electrocatalytic oxygen evolution reaction: embedded or surface-loaded. *Adv. Funct. Mater.,* 2018, ***28*** (11), 1706056.

(3) Zhang, G.; Li, Y.; Zhou, Y.; Yang, F. NiFe layered-double-hydroxide-derived NiO-$NiFe_2O_4$/reduced graphene oxide architectures for enhanced electrocatalysis of alkaline water splitting. *ChemElectroChem,* 2016, ***3*** (11), 1927–1936.

(4) Aman, S.; Ahmad, N.; Tahir, M. B.; Alanazi, M. M.; Abdelmohsen, S. A. M.; Khosa, R. Y.; Farid, H. M. T. Understanding the spatial configurations of Sm_2O_3 in NiO interfaces embedded-loaded for electrocatalytic OER process. *Surf. and Interf.* 2023, ***38*** (37), 102857.

(5) Wang, Q.; Wang, C.; Du, X.; Zhang, X. Synthesis of $NiSe_2$@M (M=Cu, Fe and Zn)–NiCo LDH with porous structure on nickel foam for overall fresh and seawater splitting. *Int. J. Hydrogen. Energy.,* 2024, ***51*** (15), 1154–1166.

(6) Zhang, C.; Li, T.; Wei, Q.; Cheng, Z.; Wu, J.; Ma, X.; Chen, Z.; Liu, K.; Zhang, T.; Liu, J. Fe-doped $NiSe_2$ nanoparticles as efficient and stable electrocatalysts for oxygen evolution reaction. *Chem. Phys. Lett.,* 2022, ***808*** (10), 140126.

(7) Liu, T.; Asiri, A. M.; Sun, X. Electrodeposited Co-doped $NiSe_2$ nanoparticles film: a good electrocatalyst for efficient water splitting. *Nanoscale,* 2016, ***8*** (7), 3911–3915.

(8) Zhou, J.; Yuan, L.; Wang, J.; Song, L.; You, Y.; Zhou, R.; Zhang, J.; Xu, J. Combinational modulations of $NiSe_2$ nanodendrites by phase engineering and iron-doping towards an efficient oxygen evolution reaction. *J. Mater. Chem. A.,* 2020, ***8*** (16), 8113–8120.

(9) Park, K. R.; Tran, D. T.; Nguyen, T. T.; Kim, N. H.; Lee, J. H. Copper-incorporated heterostructures of amorphous $NiSe_x$/crystalline $NiSe_2$ as an efficient electrocatalyst for overall water splitting. *Chem. Eng. J.,* 2021, ***422*** (77), 130048.

(10) Zhu, M.; Yan, Q.; Lu, Q.; Xue, Y.; Yan, Y.; Yin, J.; Zhu, K.; Cheng, K.; Ye, K.; Yan, J.; Cao, D.; Wang, G. Iron-doped $NiSe_2$ in-situ grown on graphene as an efficient electrocatalyst for oxygen evolution reaction. *J. Electroanal. Chem.,* 2020, ***866*** (22), 114134.

(11) Xuan, C.; Xu, Q.; Han, L.; Hou, B. Electronic structure exquisite modulation of $NiSe_2$ interface via rationally controlling Fe doping for boosting electrochemical oxygen evolution activity. *Chem. Eng. J.,* 2023, ***464*** (31), 142620.

(12) Zhou, H.; Hao, X.; Guan, J.; Deng, Y.; Wei, Z.; Liu, Y.; Zhu, G. Coordination tuning of Ni/Fe complex-based electrocatalysts for enhanced oxygen evolution. *Inorg. Chem. Front.,* 2024, ***11*** (22), 8110–8122.

(13) Shi, Y.; Zhou, S.; Liu, J.; Zhang, X.; Yin, J.; Zhan, T.; Yang, Y.; Li, G.; Lai, J.; Wang, L. An integrated amorphous cobalt phosphoselenide electrocatalyst with high mass activity boosts alkaline overall water splitting. *Appl. Catal. B.,* 2024, ***341*** (58), 123326.

(14) Cai, Z.; Zhou, D.; Wang, M.; Bak, S.; Wu, Y.; Wu, Z.; Tian, Y.; Xiong, X.; Li, Y.; Liu, W.; Siahrostami, S.; Kuang, Y.; Yang, X.; Duan, H.; Feng, Z.; Wang, H.; Sun, X. Introducing Fe^{2+} into nickel–iron layered double hydroxide: local structure modulated water oxidation activity. *Angew. Chem., Int. Ed.,* 2018, ***57*** (30), 9392–9396.

(15) Huang, Y.; Zhang, S. L.; Lu, X. F.; Wu, Z.; Luan, D.; Lou, X. W. (David). Trimetallic spinel $NiCo_{2-x}Fe_xO_4$ nanoboxes for highly efficient electrocatalytic oxygen evolution. *Angew. Chem., Int. Ed.,* 2021, ***60*** (21), 11841–11846.

(16) Xu, H.; Shan, C.; Wu, X.; Sun, M.; Huang, B.; Tang, Y.; Yan, C.-H. Fabrication of layered double hydroxide microcapsules mediated by cerium doping in metal–organic frameworks for boosting water splitting. *Energy. Environ. Sci.,* 2020, ***13*** (9), 2949–2956.

(17) Zhao, Y.; Zhang, X.; Jia, X.; Waterhouse, G. I. N.; Shi, R.; Zhang, X.; Zhan, F.; Tao, Y.; Wu, L.; Tung, C.; O'Hare, D.; Zhang, T. Sub-3 nm ultrafine monolayer layered double hydroxide nanosheets for electrochemical water oxidation. *Adv. Energy Mater.,* 2018, ***8*** (18), 1703585.

(18) Wang, J.; Gan, L.; Zhang, W.; Peng, Y.; Yu, H.; Yan, Q.; Xia, X.; Wang, X. In situ formation of molecular Ni-Fe active sites on heteroatom-doped graphene as a heterogeneous electrocatalyst toward oxygen evolution. *Sci. Adv.,* 2018, ***4*** (3), eaap7970.

(19) Li, C.; Xie, L.; Zhao, J.; Gu, L.; Tang, H.; Zheng, L.; Li, G. Interfacial Fe-O-Ni-O-Fe bonding regulates the active Ni Sites of Ni-MOFs via iron doping and decorating with FeOOH for super-efficient oxygen evolution. *Angew. Chem., Int. Ed*., 2022, **61** (17), e202116934.

(20) Li, Y.; Wu, Y.; Yuan, M.; Hao, H.; Lv, Z.; Xu, L.; Wei, B. Operando Spectroscopies Unveil Interfacial FeOOH induced highly reactive β-Ni(Fe)OOH for efficient oxygen evolution. *Appl. Catal. B.,* 2022, ***318*** (180), 121825.

(21) Xu, Z.; Tao, Y.; Sun, Z.; Bi, P.; Zhong, X.; Liao, J.; Hao, D.; Yang, L.; Xu, L.; Luo, M.; Pan, K.; Gao, Z. Ligand-engineered Ni-based metal–organic frameworks for electrochemical oxygen evolution reaction. *Chem. Eng. J.,* 2023, ***478*** (5), 147418.

(22) Xiang, Q.; Li, F.; Chen, W.; Ma, Y.; Wu, Y.; Gu, X.; Qin, Y.; Tao, P.; Song, C.; Shang, W.; Zhu, H.; Deng, T.; Wu, J. In situ vertical growth of Fe–Ni layered double-hydroxide arrays on Fe–Ni alloy foil: interfacial layer enhanced electrocatalyst with small overpotential for oxygen evolution reaction. *ACS. Energy, Lett.,* 2018, ***3*** (10), 2357–2365.

(23) Xie, J.; Xin, J.; Wang, R.; Zhang, X.; Lei, F.; Qu, H.; Hao, P.; Cui, G.; Tang, B.; Xie, Y. Sub-3 nm pores in two-dimensional nanomesh promoting the generation of electroactive phase for robust water oxidation. *Nano. Energy.,* 2018, ***53*** (113), 74–82.

(24) Li, P.; Duan, X.; Kuang, Y.; Li, Y.; Zhang, G.; Liu, W.; Sun, X. Tuning electronic structure of NiFe layered double hydroxides with vanadium doping toward high efficient electrocatalytic water oxidation. *Adv. Energy. Mater.,*

2018, ***8*** (15), 1703341.
(25) Yin, S.; Tu, W.; Sheng, Y.; Du, Y.; Kraft, M.; Borgna, A.; Xu, R. A highly efficient oxygen evolution catalyst consisting of interconnected nickel–iron-layered double hydroxide and carbon nanodomains. *Adv. Mater.,* 2018, ***30*** (5), 1705106.
(26) Ni, Y.; Shi, D.; Mao, B.; Wang, S.; Wang, Y.; Ahmad, A.; Sun, J.; Song, F.; Cao, M.; Hu, C. Under-coordinated CoFe layered double hydroxide nanocages derived from nanoconfined hydrolysis of bimetal organic compounds for efficient electrocatalytic water oxidation. *Small,* 2023, ***19*** (45), 2302556.